Wang, H. et al. (2013). Ethanol oxidation activity and structure of carbon-supported Pt-modified PdSn-Sn02 influenced by different stabilizers. Electrochimica Acta, 108: 833– 840
http://dx.doi.org/10.1016/j.electacta.2013.07.061

Ethanol oxidation activity and structure of carbon-supported Pt-modified PdSn-SnO_2 influenced by different stabilizers

Hui Wang, Ziyue Liu, Shan Ji, Keliang Wang, Tianbao Zhou and Rongfang Wang

Abstract

PdSn-SnO_2 nanoparticles supported on Vulcan XC-72 carbon were synthesized by chemical reduction in the presence of three different stabilizing agents: ethylene diamine tetra-acetic acid (EDTA), sodium citrate (Nacitrate) and hexamethylenetetramine (HMTA). TEM analysis showed that PdSn-SnO_2 /C catalyst made using the HMTA stabilizer produced the smallest particle size. XRD analysis detected the presence of PdSn alloy and the SnO_2 phase in all three PdSn-SnO_2 /C samples, and showed that PdSn-SnO_2 (HMTA) had the smallest lattice parameter. After PdSn-SnO_2 samples were modified by Pt, the particle size distribution and average size of nanoparticles of Pt-PdSn-SnO_2 did not obviously change, and the fcc structure of PdSn in all three samples was retained. XPS measurement showed a higher upshift of Pt 4f binding energy occurred for Pt/PdSn-SnO_2 /C (HMTA) compared to those of Pt/PdSn-SnO_2 /C (EDTA) and Pt/PdSn-SnO_2 /C (Nacitrate). Pt/PdSn-SnO_2 /C (HMTA) was also found to have the highest CO and ethanol oxidation activity among the three catalysts.

1. Introduction

The direct ethanol fuel cell (DEFC) affords an attractive alternative to the direct methanol fuel cell (DMFC) because: (1) ethanol is less toxic than methanol and is easier to store and transport due to its relatively higher boiling point; (2) ethanol can be produced in large quantities by chemical or biological processes; and (3) ethanol has higher energy density than methanol [1]. However, implementation of DEFC technology is hindered by the sluggish rate of the ethanol oxidation reaction (EOR) on the anode [2], and thus requires the development of effective anodic catalysts to increase EOR activity.

Recent efforts to develop anodic catalysts for EOR have mainly focused on ternary catalysts based on binary PtSn/C catalysts with various additional elements. Manthiram et al. synthesized carbon-supported PtSnPd electrocatalysts with high EOR activity promoted by oxide phases and the incorporation of Pd into PtSn/C [3]. Spinace et al. showed that substitution of some Sn by Ni resulted in increased current in all potential regions of PtSn/C while hardly shifting the onset potential [4]. They attribute the improved activity of PtSnNi/C to the modification of the electronic structure of Pt and the presence of Ni oxides. Antolini et al. showed that

PtSnRu/C with different amounts of Ru had higher EOR activity than PtSn/C, attributing this to interactions involving Sn and Ru oxides [5]. Other metals, such as Ir, In and Rh have also been incorporated into PtSn systems and found to enhance catalytic activity [2,6–8]. It should also be noted that the presence of the metal oxidized state in these systems, especially SnO_2, also improved the EOR catalytic activity in the above studies.

In the past two decades, growth of Pt overlayers (or encapsulation by Pt) on other noble metals or alloys have also attracted much attention, providing an effective method to obtain high Pt- mass-based activity at reduced cost [9]. Pt monolayers deposited on carbon-supported Sn, Ni, Ru and Rh nanoparticles have shown greatly enhanced EOR activity [10,11]. Similarly, a SnO_2 core–Pt shell structure has been reported with higher EOR activity than Pt/C and PtSn/C (E-TEK), associating with an increase in the electrochemically active surface area and an electronic effect [12].

It is clear from the above reports that a composite-core catalyst, containing alloy, SnO_2, and a Pt shell structure, affords an effective strategy to enhance catalytic activity. In this case, both the electronic effect from M and Sn in the vicinity of Pt sites, and the bifunctional mechanism from SnO_2, would provide high EOR activity and better poisoning tolerance. Hence, the aim of this work was to prepare Pt/PdSn-SnO_2/C by a sequential reduction process, and to test its performance as an EOR catalyst. The above catalyst was produced using three different stabilizers ethylene diamine tetra-acetic acid (EDTA), sodium citrate (Nacitrate) and hexamethylenetetramine (HMTA) and compared the differences in structure and EOR activity.

2. Experimental

2.1. Synthesis

PdSn-SnO_2/C catalysts, using one of the three different stabilizers, were prepared in three 100 mL flasks containing a solution of 15.6 mg of palladium chloride ($PdCl_2$), 46.2 mg of stannic chloride pentahydrate ($SnCl_4{\cdot}5H_2O$) dissolved in 30 mL of ethylene glycol (EG). Then, 401.8 mg of ethylene diamine tetraacetic acid (EDTA), 288.2 mg of sodium citrate (Nacitrate) and 250.3 mg of hexamethylenetetramine (HMTA) were added to flasks 1–3 respectively, and the solutions were stirred for 0.5 h. 100 mg of pretreated carbon black (Vulcan XC-72R) was added to the mixtures under stirring conditions with ~48 mg of sodium formate and the system adjusted to ~pH 10 by dropwise addition of a 5 wt.% KOH/EG solution. The mixture was maintained at 160 °C for 8 h. The products denoted as PdSn-SnO_2/C (EDTA), PdSn-SnO_2/C (Nacitrate) and PdSn-SnO_2/C (HMTA) were collected by filtration, washed with deionized water four times and dried in air at 60 °C for 5 h.

Pt layers formation used 0.74 mL of $H_2PtCl_6{\cdot}6H_2O$ (20 mg mL^{-1}) solution dissolved in 20 mL EG with 50 mg of the three above obtained PdSn-SnO_2/C powders

respectively, and the mixtures were stirred for 30 min, followed by addition of 7.5 mg of sodium citrate under constant stirring and adjusted pH to ~10 by the dropwise addition of a 5 wt.% KOH/EG solution. The mixtures were heated at 80 °C for 5 h. The powders were collected by filtration, washed with deionized water to remove chloride from the filtrate, followed by drying in air at 60 °C for 5 h. The Pt modified PdSn-SnO_2/C catalysts were denoted as Pt/PdSn-SnO_2/C (EDTA), Pt/PdSn-SnO_2/C (Nacitrate) and Pt/PdSn-SnO_2/C (HMTA), respectively.

2.2 Characterization

X-ray diffraction (XRD) patterns of the catalysts were recorded on a Shimadzu XD-3A diffractometer (Japan) using filtered Cu K*a* radiation. Transmission electron microscopy (TEM) measurements were carried out on a JEM-2010 Electron Microscope (Japan) with the acceleration voltage of 200 kV. The average chemical compositions of the catalyst alloy structures were determined using an IRIS advantage inductively coupled plasma atomic emission spectroscopy (ICP-AES) system (Thermo, USA). X-ray photoelectron spectroscopy (XPS) was obtained by a PHI-5702 multifunctional X-ray photoelectron spectrometer (USA).

2.3 Electrochemical measurements

Electrochemical analysis was carried out on a CHI650D electrochemical work station. A conventional three-electrode electrochemical cell was used comprising a platinum counter electrode and an Ag/AgCl (3 mol L^{-1} KCl) reference electrode. The working electrode was prepared using 5 mg of catalyst dispersed ultrasonically in 1 mL of Nafion/ethanol solution (0.25% Nafion, in volume), where 8 μL of the dispersion was transferred onto a glassy carbon (GC) disc (5 mm in diameter) using a pipette and then air dried. The solution was purged with high-purity N_2 for at least 30 min to ensure gas saturation before each measurement, and stable voltammograms recorded after 10 cycles were taken into account for all the experiments. All electrochemical measurements were carried out at ambient temperature.

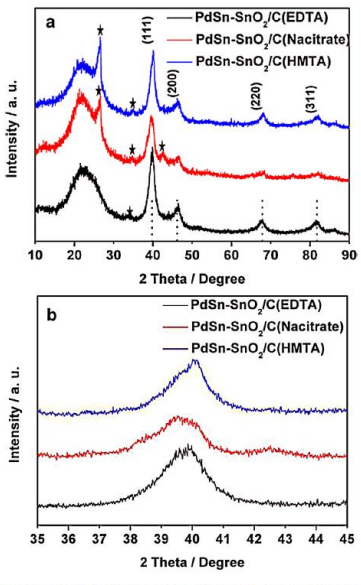

Fig. 1. The XRD patterns of PdSn-SnO_2/C (EDTA), PdSn-SnO_2/C (Nacitrate) and PdSn-SnO_2/C (HMTA) samples; and the corresponding enlarged diffraction patterns in the range of 35–45° (b).

3. Results and discussion

In the process of the formation of PdSn-SnO_2 nanoparticles, the reaction between the metal precursors, Pd^{2+} and Sn^{4+}, and the reducing agent is the primary step. At the same time, a competitive reaction to form metal complexes between metal ions and the stabilizers is occurred simultaneously. The rates of these two reactions influence the formation of particle nucleation and growth of nanoparticles as well as the composition of the alloy nanoparticles [13]. In this work, the atoms in coordination with the metal atom of EDTA, sodium citrate and HMTA is O/N, O, and N atom, respectively. Then, the competitive reaction to form metal complexes between Pd and Sn ions and the EDTA, Na citrate and HMTA is occurred differently, which results in the different characterization of PdSn-SnO_2 nanoparticles [13–16]. In the second synthesis step, the type and concentration of the stabilizer is same for the all samples. Therefore, even if the procedures of synthesizing nanoparticles are the same, the different PdSn-SnO_2 nanoparticles can lead to the different physical characterizations, then which would result in the different electrocatalytic activities.

3.1. Characterization of PdSn-SnO_2/C samples

Fig. 1 shows the crystal structure of the prepared PdSn-SnO_2 supported on carbon using the three stabilizers, EDTA, Nacitrate and HMTA, characterized by XRD. In Fig. 1a, for comparison, the XRD pattern for a prepared Pd/C sample is also plotted as the vertical dotted line. All the samples show the diffraction peak at ~24° associated with the (2 0 0) reflection of the hexagonal structure of Vulcan carbon [17], and the characteristic diffraction peaks of Pd (1 1 1) at 2e of ~40°, Pd (2 0 0) at 2e of ~46°, Pd (2 2 0) at 2e of ~67° and Pd (3 1 1) at 2e of ~81°, which has the face centred cubic (fcc) phase [18].

The reflections associated with the SnO_2 phase are located at ~26° (corresponding to the (1 1 0) plane of tetragonal SnO_2), ~34° (corresponding to the (1 0 1) plane of tetragonal SnO_2), ~52° (corresponding to the (1 1 0) plane of tetragonal SnO_2), and ~42.3° (corresponding to orthorhombic SnO_2) [19,20].

While these reflections of the SnO_2 phase were not identical, it could be concluded that SnO_2 existed in the three samples. The enlarged diffraction patterns in the range of 35–45° are presented in Fig. 1b and show that for PdSn-SnO_2/C (HMTA) the (1 1 1) diffraction peaks move to higher positions relative to that of PdSn-SnO_2/C (Nacitrate) and PdSn-SnO_2/C (EDTA), while 2e of the (1 1 1) plane for PdSn-SnO_2/C (EDTA) is slightly larger than that of PdSn-SnO_2/C (Nacitrate).

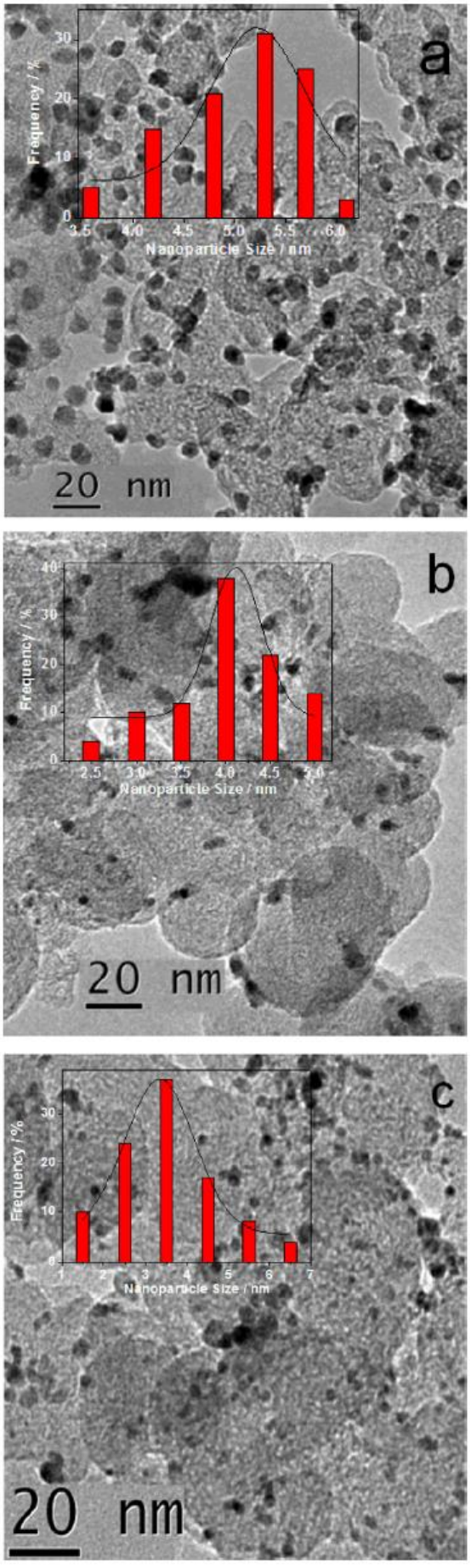

Fig. 2. (a, b and c) TEM images of PdSn-SnO_2/C (EDTA), PdSn-SnO_2/C (Nacitrate) and PdSn-SnO_2/C (HMTA) samples, respectively; and the corresponding nanoparticle size distribution histograms.

Calculated according to the literature [21], the average crystal sizes of the PdSn-SnO_2/C (EDTA), PdSn-SnO_2/C (Nacitrate) and PdSn-SnO_2/C (HMTA) samples were estimated about 5.2, 3.9 and 3.2 nm, respectively. Therefore, the different stabilizers clearly influenced the crystal sizes of PdSn-SnO_2/C samples. The lattice parameters [22] were 0.3940, 0.3942, and 0.3934 nm for the PdSn-SnO_2/C (EDTA), PdSn-SnO_2/C (Nacitrate) and PdSn-SnO_2/C (HMTA), respectively. Compared to that of Pd/C (0.3947 nm), the contraction of the Pd crystal lattice in the above samples indicates that Sn entered the crystal lattice of Pd at the atomic level to form PdSn alloy. Due to the similar size atomic radius of Sn (1.72) and Pd (1.79), the contraction was too small to observe the shift of the diffraction peak of the three samples compared to that of Pd/C.

Table 1
Composition and structural parameters of the Pt/PdSn-SnO_2/C (EDTA), Pt/PdSn-SnO_2/C (Nacitrate) and Pt/PdSn-SnO_2/C (HMTA) catalysts corresponding to a, b and c.

Catalyst	a	b	c
Compositon/Pt:Pd:Sn atom ratio	1:2.44:3.60	1:2.42:3.60	1:2.43:3.59
Mean crystalline size/nm	5.2	4.2	3.2
Lattice constant/Å	3.903 ± 0.0002	3.897 ± 0.0003	3.875 ± 0.0003
The average nanoparticle size/nm	5.2	4.2	3.3

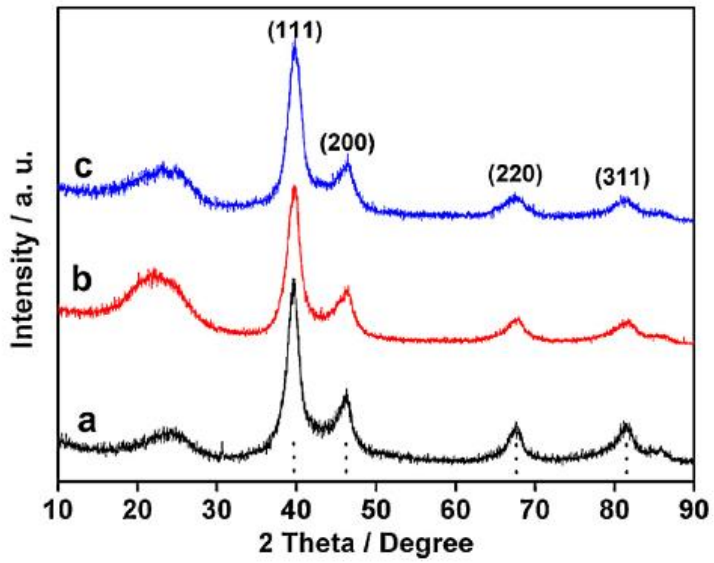

Fig. 3. The XRD patterns of the three catalysts; (a) Pt/PdSn-SnO_2/C (EDTA), (b) Pt/PdSn-SnO_2/C (Nacitrate), and (c) Pt/PdSn-SnO_2/C (HMTA).

Fig. 2 shows TEM images and corresponding particle size distributions of the three samples. For PdSn-SnO_2/C (EDTA), as noted in Fig. 2a, the dark spots of PdSn-SnO_2 nanoparticles have a spherical morphology and uniform dispersion. The nanoparticle size distribution shown as the inset in Fig. 2a is narrow with an average diameter of 5.2 nm. For PdSn-SnO_2/C (Nacitrate), particles had both elliptical and strip morphology, with uniform distribution on the carbon (see Fig. 2b), with a decrease in the size (2.5–5.0 nm) compared to that of the PdSn-SnO_2/C (EDTA) sample, with an average diameter of 4.2 nm. For PdSn-SnO_2/C (HMTA), Fig. 2c, the PdSn-SnO_2

nanoparticles were uniformly dispersed on the carbon with irregular spherical shape from 1.5 to 6.5 nm and average diameter of 3.3 nm.

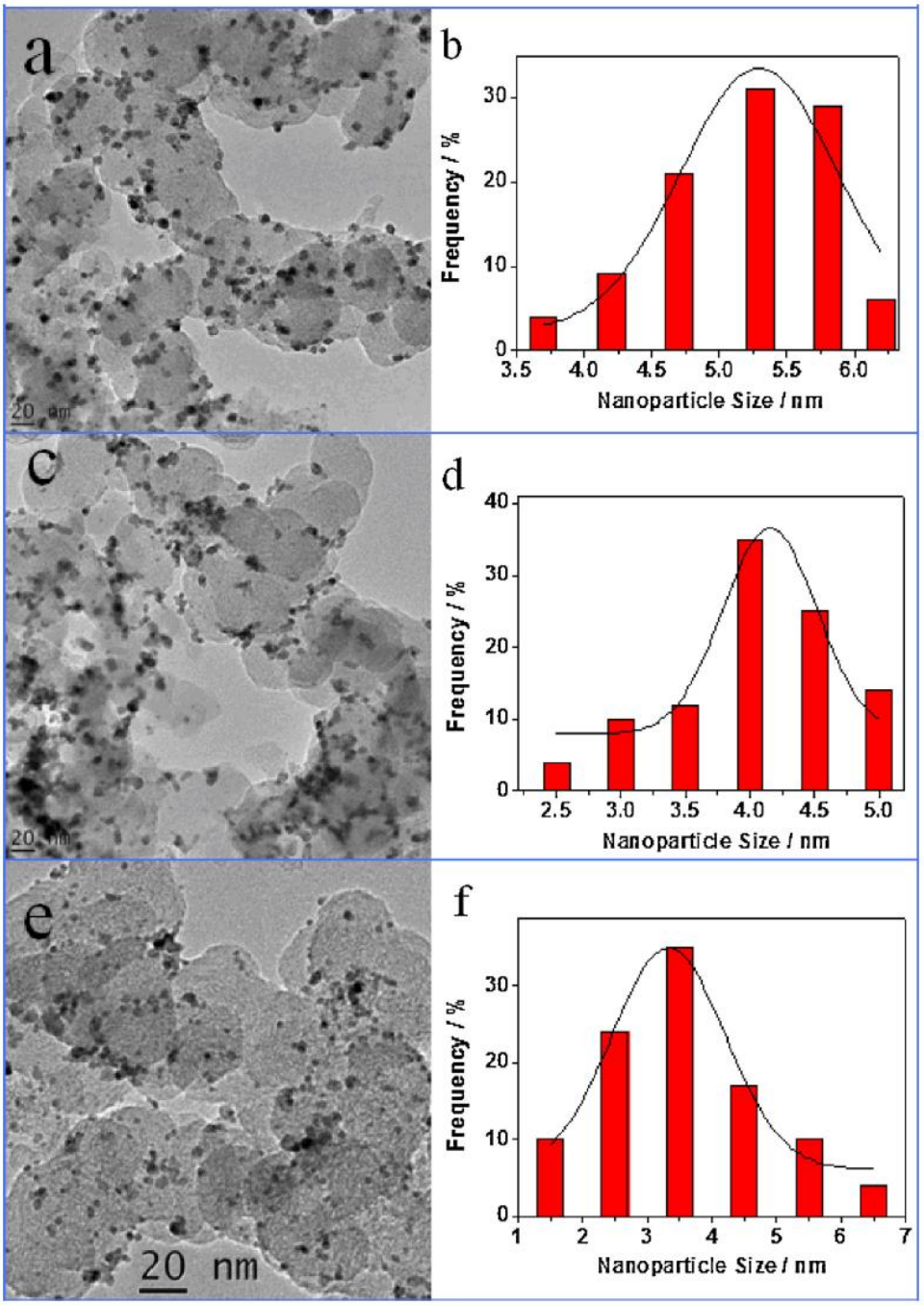

Fig. 4. TEM images and the corresponding nanoparticle size distribution histograms of Pt/PdSn-SnO_2/C (EDTA) (a and b), Pt/PdSn-SnO_2/C (Nacitrate) (c and d) and Pt/PdSn-SnO_2/C (HMTA) (e and f).

It should be noted that the average nanoparticle size stated was a rough estimation due to the irregular shape of the nanoparticles, especially for the PdSn-SnO2/C (Nacitrate) sample.

3.2. Characterization of Pt/PdSn-SnO_2/C catalysts

The chemical compositions of the three Pt/PdSn-SnO_2/C catalysts were evaluated by ICP, listed in Table 1. Based on the concentration of each element, metallic loading was ca. 24 wt.% for the three catalysts.

Fig. 3 shows the XRD patterns of the three Pt/PdSn-SnO_2/C catalysts. For comparison, the diffraction peak of prepared Pt/C was also plotted as the vertical dotted line. All the samples show the diffraction peak associated with the (2 0 0) plane of Vulcan carbon, and the characteristic diffraction peaks of Pt (1 1 1), (2 0 0), (2 2 0) and (3 1 1), which was present in the fcc phase [23]. For all the catalysts, no diffraction peak related to SnO_2 was found. This was because either some SnO_2 was chemically reduced in the second step of the synthesis procedure, or that the Pt layers on SnO_2 nano-islands had weakened the signals from SnO_2. However, the presence of SnO_2 in the three Pt/PdSn-SnO_2/C catalysts was later supported by XPS data.

In addition, compared to the diffraction of home-made Pt/C, the (1 1 1) diffraction peak of the three catalysts slightly shifted towards higher 2e values, implying that the crystal lattice of Pt (see Table 1) contracted, which might originate from the strain effect of the core on the Pt layer. Here, the compressive strain shortens the Pt Pt bonds causing d orbital to overlap to a larger degree. Since the d-band of Pt is more than half-filled, the broadening d-band would be expected to result in a downshift in the centre of gravity of the d-band compared to the Fermi level for maintaining constant filling and conserving energy [24,25]. This evidence could also be supported by the following XPS results. On the other hand, the average crystal sizes according to the literature [24] of the three catalysts were estimated and shown in Table 1. A similar average crystal size between the Pt/PdSn-SnO_2/C catalysts and the PdSn-SnO_2/C samples was observed, suggesting the Pt layers were thin.

Fig. 4 shows the TEM images of the three Pt/PdSn-SnO_2/C catalysts and the corresponding particle size distribution histograms. The Pt/PdSn-SnO_2 nanoparticles were well dispersed on the surface of the support with a narrow particle size distribution for the three catalysts. In Table 1, the average nanoparticle size of Pt/PdSn-SnO_2/C (EDTA), Pt/PdSn-SnO_2/C (Nacitrate) and Pt/PdSn-SnO_2/C (HMTA) catalyst does not obviously increase compared to their non-platinized states, suggesting the Pt layer was thin.

Fig. 5 shows the narrow scan of Pt 4f core level of XPS of the three catalysts. The spectra show a doublet containing a low energy band ($4f_{7/2}$) and a high energy band ($4f_{5/2}$), which are listed in Table 2. Here, the Pt 4f binding energy of the prepared Pt/C catalyst is also listed for comparison [26]. For the three Pt/PdSn-SnO_2/C catalysts, the Pt 4f binding energy gave a positive shift compared to Pt/C. In Pt/PdSn-SnO_2/C catalysts, the PdSn-SnO_2 core with the smaller lattice parameter introduces strain effects on the Pt shell with the larger lattice parameter [27,28]. The squeezed Pt atoms lead to the increased overlap of the d orbital, and

consequently the band broadens. In order to maintain the same filling degree, the centre of the d-band moves to low energy, resulting in the increase of Pt XPS binding energies, such a phenomenon has been previously suggested [26,29,30].

Table 2
The binding energies of Pt 4f of the three catalysts.

Catalyst	Pt $4f_{7/2}$	Pt $4f_{5/2}$
Pt/PdSn-SnO_2/C (EDTA)	71.8	75.0
Pt/PdSn-SnO_2/C (Nacitrate)	71.7	75.0
Pt/PdSn-SnO_2/C (HMTA)	72.0	75.2
Pt/C [26]	71.3	74.6

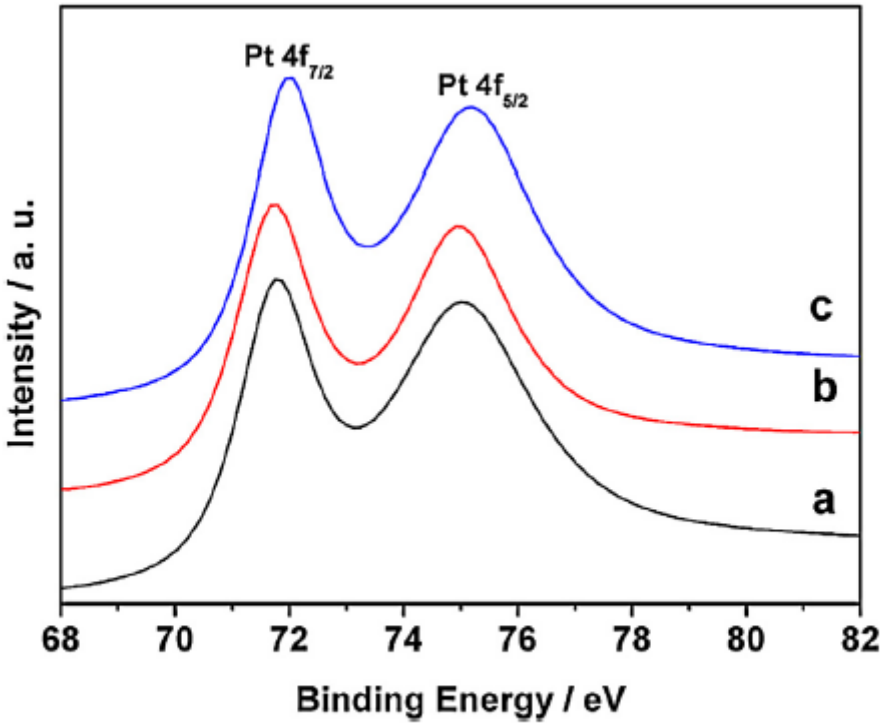

Fig. 5. XPS of Pt 4f of the three catalysts; (a) Pt/PdSn-SnO_2/C (EDTA), (b) Pt/PdSn-SnO_2/C (Nacitrate), and (c) Pt/PdSn-SnO_2/C (HMTA).

Furthermore, the stronger strain effect results in the larger shift of Pt XPS binding energy, demonstrated by the consistency between the XPS results and the above XRD results. The upward shifts of the Pt 4f binding energy in Pt/PdSn-SnO_2/C catalysts follows in the order Pt/PdSn-SnO_2/C (EDTA) ≈ Pt/PdSn-SnO_2/C (Nacitrate) < Pt/PdSn-SnO_2/C (HMTA), implying that the d-band centre value in Pt/PdSn-SnO_2/C (HMTA) catalyst is lower than that of other two catalysts.

The Sn 3d XPS spectra for the three catalysts are shown in Fig. 6. At a glance, the Sn 3d region is more complicated than that of the Pt 4f region. In order to better understand the contribution of different forms of Sn atoms to the different catalysts, deconvolution of XPS Sn 3d peaks was carried out. According to the literature [31–33], the Sn 3d spectrum was deconvoluted using two components, one for Sn(0) and

the second for Sn(IV). For Pt/PdSn-SnO_2/C (EDTA), the Sn $3d_{5/2}$ binding energy components are fixed at 485.3 and 486.8 eV (see Table 3), as well as 8.3 eV spin–orbit splitting. The XPS signal at 485.3 eV can be attributed to Sn(0) and that at 486.8 eV to SnO_2 [31,32,34]. The result supports the presence of SnO_2 in Pt/PdSn-SnO_2/C (EDTA) catalyst, which was not discernible previously by XRD analysis. From Fig. 6a, the prevailing occurrence of Sn(IV) in the PdSn-SnO_2 core of the Pt/PdSn-SnO_2/C (EDTA) catalyst, and a atom fraction of Sn(IV) was ca. 68%.

The results of the deconvolution of Pt/PdSn-SnO_2/C (Nacitrate) and Pt/PdSn-SnO_2/C (HMTA) catalysts are also summarized in Table 3. It is evident that, after modification of the PdSn-SnO_2 nanoparticles with the Pt layer, SnO_2 was the predominate form of Sn in the three catalyst. The oxidized forms account for about 55% of the total Sn atom in Pt/PdSn-SnO_2/C (HMTA), which was lower than that of the other two catalysts.

3.3. Electrochemical performance of Pt/PdSn-SnO_2/C catalysts

Fig. 7 shows cyclic voltammetry (CV) results for the oxidation of a monolayer of pre-adsorbed CO (CO stripping voltammograms) obtained for the three catalysts. For clarity, the first scan is shown as a black solid line and the second scan as a red dotted line. A clean surface is recovered in the second cycle coinciding with the voltammogram in the base electrolyte. Common behaviour described in the literature [35] was observed for the three catalysts.

Table 3
The binding energies of Sn $3d_{5/2}$ of the three catalysts.

Catalyst	Sn $3d_{5/2}$/eV		The fraction of Sn(IV)/%
	Sn(0)	Sn(IV)	
Pt/PdSn-SnO_2/C (EDTA)	485.3	486.8	68
Pt/PdSn-SnO_2/C (Nacitrate)	485.3	486.9	63
Pt/PdSn-SnO_2/C (HMTA)	485.6	487.0	55

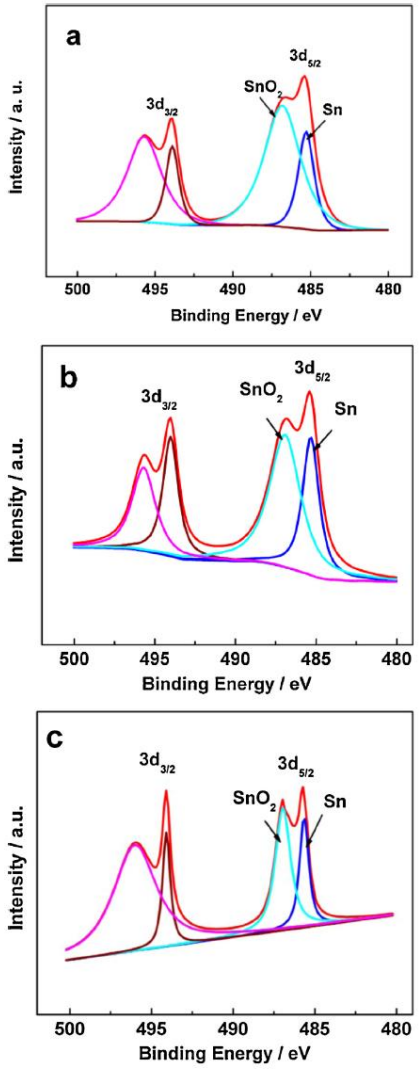

Fig. 6. XPS of Sn 3d of the three catalysts; (a) Pt/PdSn-SnO_2/C (EDTA), (b) Pt/PdSn-SnO_2/C (Nacitrate), and (c) Pt/PdSn-SnO_2/C (HMTA).

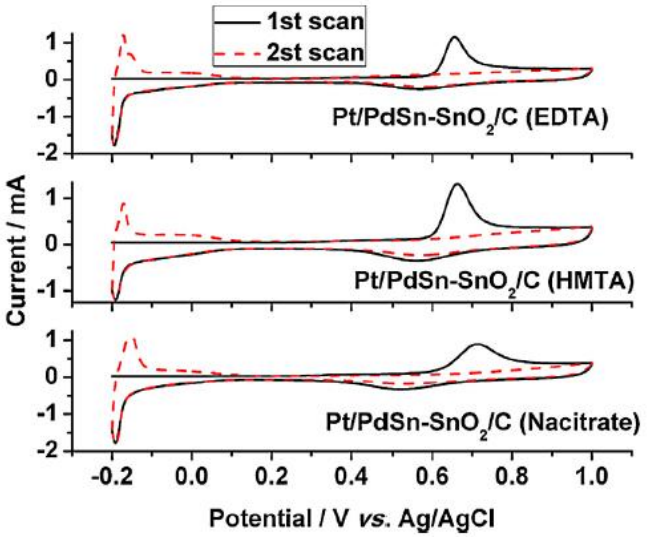

Fig. 7. CO stripping voltammograms in 0.5 mol L^{-1} H_2SO_4 of the Pt/PdSn-SnO_2/C (EDTA), Pt/PdSn-SnO_2/C (Nacitrate), and Pt/PdSn-SnO_2/C (HMTA) catalysts, at a potential scan rate of 50 mV s^{-1}.

From Fig. 7, the CO stripping peak potential of the Pt/PdSn-(EDTA) catalyst was almost the same as that of the Pt/PdSn-SnO_2/C (HMTA) catalyst, while the CO stripping peak potential of both of the Pt/PdSn-SnO_2/C (EDTA) and Pt/PdSn-SnO_2/C (HMTA) catalysts were more positive than that of Pt/PdSn-SnO_2/C (Nacitrate), which could be mainly attributed to strain effects. The d-band centre value of Pt in Pt/PdSn-SnO_2/C catalysts was in the order Pt/PdSn-SnO_2/C (HMTA) < Pt/PdSn-SnO_2/C (EDTA) < Pt/PdSn-SnO_2/C (Nacitrate). Here, in correlation with previous reports, Pt surface with a low d-band centre value binds CO more weakly, facilitating CO oxidation [26,36,37]. So, CO oxidation on the Pt/PdSn-SnO_2/C (HMTA) and Pt/PdSn-SnO_2/C (EDTA) electrodes is easy compared to the Pt/PdSn-SnO_2/C (Nacitrate) electrode.

The electrochemically surface area (*ECSA*) of the catalyst is calculated using the equation [37]:

$$ECSA = \frac{Q_{CO}}{420 W_{Pt}}$$

where *ECSA* is the electrochemical active surface area of different catalysts, Q_{CO} is the charge for CO desorption electro-oxidation in microcoulomb (μC) after subtracting the charge from the 2nd scan region, 420 is the charge required to oxidize a monolayer of CO on the catalyst in μC cm^{-2}, and *W* is the Pd and Pt loading.

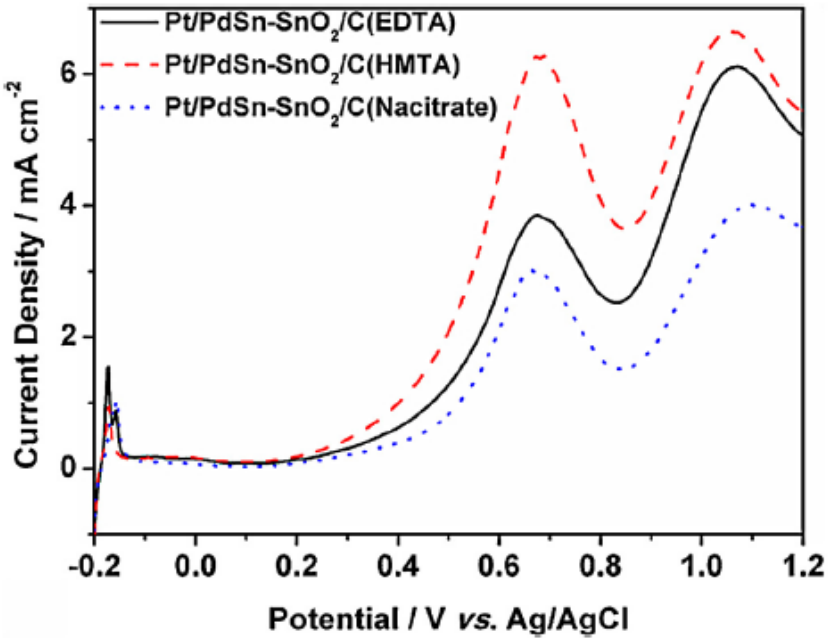

Fig. 8. Linear scan voltammetry in 0.5 mol L^{-1} H_2SO_4 + 0.5 mol L^{-1} C_2H_5OH–N_2 purged solution with a potential scan rate of 50 mV s^{-1} recorded at the three catalysts' electrodes.

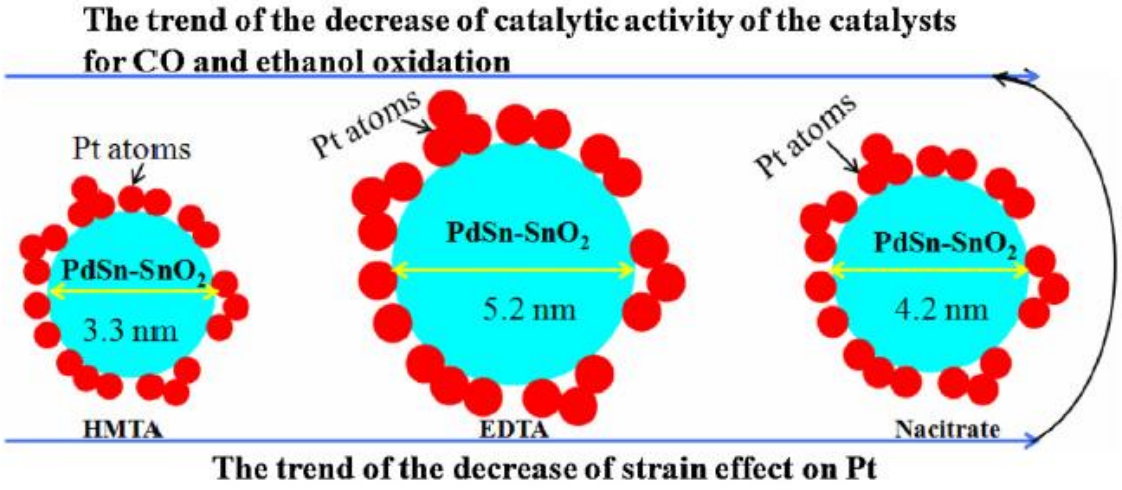

Fig. 9. Diagram for the trend of the catalytic activity of the three catalysts.

The results of ECSA are 27.8, 23.0, and 24.4 m^2 $g_{preciou\ metal}^{-1}$ for Pt/PdSn-SnO_2/C (HMTA), Pt/PdSn-SnO_2/C (EDTA) and Pt/PdSn-SnO_2/C (Nacitrate) respectively. This result demonstrates that Pt/PdSn-SnO_2/C (HMTA) has more active sites compared with the Pt/PdSn-SnO_2/C (EDTA) and Pt/PdSn-SnO_2/C (Nacitrate) catalysts, which relates to the particle size of Pt/PdSn-SnO_2/C (HMTA) being smaller than that of the other two catalysts.

The EOR activity of the three Pt/PdSn-SnO_2/C catalysts was characterized by anodic sweep cyclic voltammetry (Fig. 8) where the current was normalized for the *ECSA* of the electrode. The current density of two oxidation peaks for Pt/PdSn-SnO_2/C (HMTA) was 6.3 and 6.7 mA cm^{-2} at nearly 0.68 and 1.06 V, respectively, significantly higher than those of Pt@PdSn-SnO_2/C (EDTA) (3.8 and 6.1 mA cm^{-2} at ca. 0.67 and 1.06 V, respectively) and Pt/PdSn-SnO_2/C (Na citrate) (3.0 and 4.0 mA cm^{-2} at ca. 0.67 and 1.09 V, respectively). The higher current density for Pt/PdSn-SnO_2/C (HMTA) indicates that its performance was superior to Pt/PdSn-SnO_2/C (EDTA) and Pt/PdSn-SnO_2/C (Nacitrate) [38]. In addition, the Pt/PdSn-SnO_2/C (EDTA) catalyst also had higher catalytic activity than the Pt/PdSn-SnO_2/C (Nacitrate) catalyst.

On the basis of the above results, we have shown how different stabilizers affect the distribution and structure of the Pt/PdSn-SnO_2/C catalysts and produce different levels of EOR activity (illustrated as Fig. 9), which we attribute mainly to the strain effect. While the particle size [39,40] and the extent of Sn oxidation [33] may exert an influence on the catalytic activity of Pt/PdSn-SnO_2/C catalysts, this does not explain why Pt/PdSn-SnO_2/C (EDTA) had higher CO and EOR activity than Pt/PdSn-SnO_2/C (Nacitrate).

4. Conclusions

PdSn-SnO_2 nanoparticles supported on Vulcan XC-72 carbon were successfully synthesized using different stabilizers, and modified with Pt layer. Pt/PdSn-SnO_2/C (HMTA) catalyst produced well-separated, smaller, particles (2.2 nm) than those of Pt/PdSn-SnO_2/C (EDTA) and Pt/PdSn-SnO_2/C (Nacitrate), with all three catalysts showing the fcc phase for Pt, PdSn alloy and SnO_2 phase. XPS measurements showed the order of the strain effect to be: Pt/PdSn-SnO_2/C (HMTA) > Pt/PdSn-SnO_2/C (EDTA) > Pt/PdSn-SnO_2/C (Nacitrate). The cyclic voltammetric response for CO and EOR activity revealed that the surface area and the EOR current of the Pt/PdSn-SnO_2/C (HMTA) catalyst was higher than that of the other two catalysts, due to the stronger strain effect on Pt.

Acknowledgments

The authors would like to thank the National Natural Science Foundation of China (21163018), the National Science Foundation for Post-doctoral Scientists of China (20110490847, 2012T50554) and Guangdong Key Lab for Fuel Cell Technology for financially supporting this work.

References

[1] W. Du, Q. Wang, D. Saxner, N.A. Deskins, D. Su, J.E. Krzanowski, A.I. Frenkel, X. Teng, Highly active Iridium/Iridium–Tin/Tin oxide heterogeneous nanoparticles as alternative electrocatalysts for the ethanol oxidation reaction, Journal of the American Chemical Society 133 (2011) 15172.

[2] M. Zhu, G. Sun, S. Yan, H. Li, Q. Xin, Preparation, structural characterization, and activity for ethanol oxidation of carbon-supported PtSnIn catalyst, Energy
& Fuels 23 (2009) 403.

[3] E. Lee, I.S. Park, A. Manthiram, Synthesis and characterization of Pt–Sn–Pd/C catalysts for ethanol electro-oxidation reaction, Journal of Physical Chemistry C 114 (2010) 10634.

[4] E.V. Spinacé, M. Linardi, A.O. Neto, Co-catalytic effect of nickel in the electro-oxidation of ethanol on binary Pt-Sn electrocatalysts, Electrochemistry Communications 7 (2005) 365.

[5] Y.W. Chang, C.W. Liu, Y.C. Wei, K.W. Wang, Promotion of PtRu/C anode catalysts for ethanol oxidation reaction by addition of Sn modifier, Electrochemistry Communications 11 (2009) 2161.

[6] J. Ribeiro, D.M. dos Anjos, K.B. Kokoh, C. Coutanceau, J.M. Léger, P. Olivi, A.R. de Andrade, G. Tremiliosi-Filho, Carbon-supported ternary PtSnIr catalysts for direct ethanol fuel cell, Electrochimica Acta 52 (2007) 6997.

[7] W. Du, Q. Wang, C.A. LaScala, L. Zhang, D. Su, A.I. Frenkel, V.K. Mathur, X. Teng, Ternary PtSnRh–SnO_2 nanoclusters: synthesis and electroactivity for ethanol oxidation fuel cell reaction, Journal of Materials Chemistry 21 (2011) 8887.

[8] J.C. Castro, R.M. Antoniassi, R.R. Dias, M. Linardi, E.V. Spinacé, A.O. Neto, Preparation of PtSnRh/C-Sb_2O_5 ·SnO_2 electrocatalysts by an alcohol reduction process for direct ethanol fuel cell, Ionics 18 (2012) 781.

[9] H.L. Jiang, Q. Xu, Recent progress in synergistic catalysis over heterometallic nanoparticles, Journal of Materials Chemistry 21 (2011) 13705.

[10] F.H.B. Lima, E.R. Gonzalez, Electrocatalysis of ethanol oxidation on Pt mono-layers deposited on carbon-supported Ru and Rh nanoparticles, Applied Catalysis B: Environmental 79 (2008) 341.

[11] G. Li, P.G. Pickup, Decoration of carbon-supported Pt catalysts with Sn to promote electro-oxidation of ethanol, Journal of Power Sources 173 (2007) 121.

[12] J.C.M. Silva, R.F.B. De Souza, L.S. Parreira, E.T. Neto, M.L. Calegaro, M.C. Santos, Ethanol oxidation reactions using SnO_2 @Pt/C as an electrocatalyst, Applied Catalysis B: Environmental 99 (2010) 265.

[13] F. Somodi, Z. Peng, A.B. Getsoian, A.T. Bell, Effects of the synthesis parameters on the size and composition of Pt–Sn nanoparticles prepared by the polyalcohol reduction method, Journal of Physical Chemistry C 115 (2011) 19084.

[14] X. Wang, J. Stover, V. Zielasek, L. Altmann, K. Thiel, K. Al-Shamery, M. Baumer,
H. Borchert, J. Parisi, J. Kolny-Olesiak, Colloidal synthesis and structural control of PtSn bimetallic nanoparticles, Langmuir 27 (2011) 11052.

[15] Z. Liu, D. Reed, G. Kwon, M. Shamsuzzoha, D.K. Nikles, Pt3 Sn nanoparticles with controlled size: high-temperature synthesis and room-temperature catalytic activation for electrochemical methanol oxidation, Journal of Physical Chemistry C 111 (2007) 14223.
[16] X. Wang, L. Altmann, J. Stöver, V. Zielasek, M. Bäumer, K. Al-Shamery, H. Borchert, J. Parisi, J. Kolny-Olesiak, Pt/Sn intermetallic, core/shell and alloy nanoparticles: colloidal synthesis and structural control, Chemistry of Materials 25 (2013) 1400.
[17] Z. Lei, Pt overgrowth on carbon supported PdFe seeds in the preparation of core–shell electrocatalysts for the oxygen reduction reaction, Journal of Power Sources 195 (2010) 3498.
[18] J.C. Jia, R.F. Wang, H. Wang, S. Ji, J. Key, V. Linkov, K. Shi, Z.Q. Lei, A novel structural design of CNx-Fe3 O4 as support to immobilize Pd for catalytic oxidation of formic acid, Catalysis Communications 16 (2011) 60.
[19] Ü. Kersen, L. Holappa, H2 S-sensing properties of SnO2 produced by ball milling and different chemical reactions, Analytica Chimica Acta 562 (2006) 110.
[20] M.R. Yang, S.Y. Chu, R.C. Chang, Synthesis and study of the SnO2 nanowires growth, Sensors and Actuators B – Chemical 122 (2007) 269.
[21] Z. Liu, X. Zhang, Carbon-supported PdSn nanoparticles as catalysts for formic acid oxidation, Electrochemistry Communications 11 (2009) 1667.
[22] V. Radmilovic, H.A. Gasteiger, P.N. Ross Jr., Structure and chemical composition of a supported Pt-Ru electrocatalyst for methanol oxidation, Journal of Catalysis 154 (1995) 98.
[23] R. Wang, X. Li, H. Li, Q. Wang, H. Wang, W. Wang, J. Kang, Y. Chang, Z. Lei, Highly stable and effective Pt/carbon nitride (CNx) modified SiO2 electrocatalyst for oxygen reduction reaction, International Journal of Hydrogen Energy 36 (2011) 5775.
[24] M.K. Jeon, K.R. Lee, S.I. Woo, Enhancement in electro-oxidation of methanol over PtRu black catalyst through strong interaction with iron oxide nanocluster, Langmuir 26 (2010) 16529.
[25] M.A. Rigsby, W.P. Zhou, A. Lewera, H.T. Duong, P.S. Bagus, W. Jaegermann, R. Hunger, A. Wieckowski, Experiment and theory of fuel cell catalysis: Methanol and formic acid decomposition on nanoparticle Pt/Ru, Journal of Physical Chemistry C 112 (2008) 15591.
[26] X. Zhang, H. Wang, J. Key, V. Linkov, S. Ji, X. Wang, Z. Lei, R. Wang, Strain effect of core-shell Co@Pt/C nanoparticle catalyst with enhanced electrocatalytic activity for methanol oxidation, Journal of the Electrochemical Society 159 (2012) B270.
[27] T. Bligaard, J.K. Nørskov, Ligand effects in heterogeneous catalysis and electrochemistry, Electrochimica Acta 52 (2007) 5512.
[28] J.X. Wang, H. Inada, L. Wu, Y. Zhu, Y. Choi, P. Liu, W.-P. Zhou, R.R. Adzic, Oxygen reduction on well-defined core–shell nanocatalysts: particle size, facet, and Pt shell thickness effects, Journal of the American Chemical Society 131 (2009) 17298.

[29] M. Garciacontreras, S. Fernandezvalverde, J. Vargasgarcia, M. Cortesjacome, J. Toledoantonio, C. Angeleschavez, Pt, PtCo and PtNi electrocatalysts prepared
by mechanical alloying for the oxygen reduction reaction in 0.5 M H_2SO_4 , International Journal of Hydrogen Energy 33 (2008) 6672.
[30] G. Chen, D. Xia, Z. Nie, Z. Wang, L. Wang, L. Zhang, J. Zhang, Facile synthesis of Co–Pt hollow sphere electrocatalyst, Chemistry of Materials 19 (2007) 1840.
[31] S.C. Zignani, E.R. Gonzalez, V. Baglio, S. Siracusano, A.S. Aricò, Investigation of a Pt_3Sn/C electro-catalyst in a direct ethanol fuel cell operating at low temperatures for portable applications, International Journal of Electrochemical Science 7 (2012) 3155.
[32] H.J. Ahn, K.W. Park, Y.E. Sung, Synthesis and characterization of Sn nanophases in a Ta_2O_5 matrix, Chemistry of Materials 16 (2004) 1991.
[33] A. Lewera, P.J. Barczuk, K. Skorupska, K. Miecznikowski, M. Salamonczyk,
P.J. Kulesza, Influence of polyoxometallate on oxidation state of tin in Pt/Sn nanoparticles and its importance during electrocatalytic oxidation of ethanol
– Combined electrochemical and XPS study, Journal of Electroanalytical Chemistry 662 (2011) 93.
[34] J. Yang, H. Zhao, F. Zhang, Effects of heat treatment on the chemical states of O1s and Sn3d at the surface of SnO_X:F films by APCVD, Materials Letters 90 (2013) 37.
[35] J.R.C. Salgado, J.J. Quintana, L. Calvillo, M.J. Lazaro, P.L. Cabot, I. Esparbe, E. Pastor, Carbon monoxide and methanol oxidation at platinum catalysts supported on ordered mesoporous carbon: the influence of functionalization of the support, Physical Chemistry Chemical Physics 10 (2008) 6796.
[36] H. Wang, H. Da, S. Ji, S. Liao, R. Wang, Selenium-functionalized carbon as a support for platinum nanoparticles with improved electrochemical properties for the oxygen reduction reaction and CO tolerance, Journal of the Electrochemical Society 160 (2013) H266.
[37] R.F. Wang, B.X. Wei, H. Wang, S. Ji, J. Key, X.T. Zhang, Z.Q. Lei, An effective electrocatalyst for ethanol oxidation: Pt-modified IrCu alloy nanoparticle, Ionics 17 (2011) 595.
[38] H. Wang, X. Zhang, R. Wang, S. Ji, W. Wang, Q. Wang, Z. Lei, Amorphous CoSn alloys decorated by Pt as high efficiency electrocatalysts for ethanol oxidation, Journal of Power Sources 196 (2011) 8000.
[39] J. Prabhuram, X. Wang, C.L. Hui, I.-M. Hsing, Synthesis and characterization of surfactant-stabilized Pt/C nanocatalysts for fuel cell applications, Journal of Physical Chemistry B 107 (2003) 11057.
[40] W.F. Chen, H.Y. Huang, C.H. Lien, P.L. Kuo, Enhanced stabilization and depo-bell-like polyethyleniminated poly(oxypropylene)diamine, Journal of Physical Chemistry B 110 (2006) 9822.